Hindawi
Advances in Condensed Matter Physics
Volume 2024, Article ID 6613380, 13 pages
https://doi.org/10.1155/2024/6613380

Research Article

Enhancement in the Electrocatalytic and Optoelectronic Performance of Cost-Effective Counter Electrode VO_2 for Dye-Sensitized Solar Cell (DSSC)

Varsha Yadav,[1] **Rahul Bhatnagar**,[2] **and Upendra Kumar**[3]

[1]*School of Applied Science, Shri Venkateshwara University, Gajraula (Amroha) 244221, U.P., India*
[2]*School of Engineering and Technology, Shri Venkateshwara University, Gajraula (Amroha) 244221, U.P., India*
[3]*Advanced Functional Materials Laboratory, Department of Applied Science, Indian Institute of Information Technology Allahabad, Prayagraj-211015, U.P., India*

Correspondence should be addressed to Upendra Kumar; upendrakumar@iiita.ac.in

Received 31 October 2023; Revised 23 November 2023; Accepted 12 December 2023; Published 16 January 2024

Academic Editor: Tholkappiyan Ramachandran

Dye-sensitized solar cells (DSSCs) have garnered significant attention in the scientific community for more than two decades due to their cost-effectiveness, convenient manufacturability, little toxicity, and straightforward preparation methodology. In this study, we present a cost-effective alternative to the platinum electrode for DSSCs, which serves as the counter electrode. The utilization of vanadium oxide nanoparticles as counter electrodes (CEs) in DSSCs has been the subject of research due to its enhanced stability, cost-effectiveness, and favorable photovoltaic characteristics. The device has been fabricated in configuration of fluorine-doped tin oxide (FTO)||TiO_2||ruthenium (II) dye (N719)||iodide—triiodide electrolyte||VO_2 (counter electrode)||FTO and investigate their photovoltaic performance. The utilization of X-ray diffraction (XRD) analysis has provided insights into the crystalline properties of VO_2, indicating that it exists in a crystalline phase with a crystalline size measuring 43.19 nm and a lattice strain of 1.68×10^{-3}. The utilization of a field emission scanning electron microscope (FESEM) that is equipped with an energy dispersive X-ray spectrum reveals a dense microstructure characterized by a uniform distribution of vanadium (V) and oxygen (O) across the whole surface. The Raman spectroscopic examination of VO_2 reveals the existence of many Raman bands, thereby confirming the presence of the monoclinic phase. Cyclic voltammetry measurements were employed to investigate the catalytic activity of the CE toward the electrolyte. The photovoltaic performance of the manufactured device was examined by I–V measurement, revealing a notable open circuit voltage (Voc) and efficient power conversion efficiency when compared to the other materials that were evaluated.

1. Introduction

The present solar technologies are mostly based on the use of crystalline silicon and cadmium telluride materials. Various challenges and issues pertaining to contemporary technology are associated with these materials. More than 90% of the currently available photovoltaic systems (PVs) are comprised of silicon-based solar cells [1]. These solar cells have a life span of approximately 15–20 years and possess a relatively high-power conversion efficiency (PCE) of roughly 27%. The primary challenge faced by the photovoltaic (PV) sector pertains to the cost to electricity output ratio of solar-generated electricity. Unfortunately, none of the aforementioned options are capable of resolving this issue [2]. Additionally, some of these PVs' high-energy costs to manufacture negate any environmental advantages. This development paves the way for the establishment of a more tangible system that is economically viable in providing the necessary infrastructure for solar energy harvesting [3]. The utilization of TiO_2-based dye-sensitized solar cells (DSSCs) is deemed as a suitable option for providing a resolution to this issue. The claim that photovoltaics (PVs) is the most efficient material system for enabling a reliable mechanism for large-scale solar harvesting is supported by the combination of affordable material costs and the ability to establish cost-effective production facilities that can be readily deployed. This allows for

straightforward fabrication methods and limited environmental impact in terms of energy consumption and utilization of sustainable materials [4, 5].

DSSCs represent a promising "emerging technology" categorized as a third-generation photovoltaic (PV) system, which holds potential as a cost-effective alternative for energy conversion when compared to the existing methodologies. In the last 20 years, DSSCs have achieved significant advancements in both fundamental research and practical technological implementation [6]. The assertion that photovoltaic's (PVs) presents an optimal material system for efficient large-scale solar energy collection is well-substantiated by the convergence of affordable materials and cost-effective production facilities that can be easily implemented through solution-based processes. These aspects enable the use of uncomplicated manufacturing techniques and contribute to a reduced ecological footprint in terms of energy usage during production and the utilization of eco-friendly materials. The attainment of long-term dependability standards can be accomplished through the integration of an appropriate nanomaterial inside the roll-to-roll manufacturing technique employed for flexible devices. This integration ensures the provision of enough mechanical strength and flexibility [7, 8]. The notion of DSSCs in plants was derived from the photosynthesis process, in which the absorption of sunlight by chlorophyl, an organic molecule, triggers the initiation of photosynthesis. The primary concern of DSSCs was instability, however, the discovery of the photovoltaic effect in DSSCs dates back to the early 1970s. Despite the subsequent rise in efficiency, the persistent problem of inadequate stability continued to pose a significant concern [9, 10]. At present, there are ongoing efforts to make improvements to DSSC in order to improve its photovoltaic efficiency. The experimental setup involves the connection of two electrodes, specifically a semiconductor photoanode acting as the anode and a counter electrode serving as the cathode, to opposite ends of a liquid electrolyte containing a redox pair. Titanium dioxide (TiO_2) is commonly utilized as a photoanode semiconductor material due to its notable attributes, such as its abundant availability, stability, low toxicity, and wide band gap [11, 12]. Enhancing the overall photovoltaic efficiency of DSSCs can be achieved by this approach, yielding positive outcomes. Nanomaterials also have a significant impact on DSSCs, specifically in the context of cathode electrode foams serving as counter electrodes. A catalyst material is used as a counter electrode directly for two key reasons: (a) It collects the electrons from the external load and transfers them to the electrolyte and (b) It plays the role of catalyst, which is beneficial for the generation of the redox couple [13]. The efficiency and cost of the final solar cell are determined by each individual component of the device. One of the challenges associated with DSSC technology pertains to the difficulty in identifying a suitable substitute for the Pt electrode, given its composition of a valuable metal. Platinum (Pt) is considered a favored catalyst material in the field of chemical engineering due to its exceptional electrocatalytic properties and high-electrical conductivity. Certain findings suggest that platinum (Pt) undergoes a reaction with triiodide ions (I^{3-}) present in the electrolyte, resulting in the formation of platinum tetraiodide (PtI_4). This reaction subsequently diminishes the catalytic activity of the electrode when exposed to a dye solution [14]. Thus, an alternative to the CEs will be found to overcome these issues. Thus, many researchers explore platinum-free material as a promising alternative to Pt for a counter electrode. The number of reports on alternate CEs has grown exponentially [15].

Among them, the work reported by Xia et al. [16] prepared the composite electrode of V_2O_5 with Al and applied it in DSSC as the CE. They had achieved a PCE of 2% which is comparable to noble Ag CE (generally used in solid DSC) [16]. Alternatively, Mutta et al. [17] investigated the economically viable VO_2 (M1) as a CE for DSSC. They had found that VO_2 improved the electrocatalytic behavior of the redox reaction between iodide and triiodide reactions, which might work as a substitute for expensive Pt electrodes due to their low cost, low-temperature processing, and excellent catalytic activity. Moreover, they reduced the cost of CE, but their efficiency is only about 1.25% Alternatively, Mutta et al. [17] investigated the economically viable VO_2 (M1) as a CE for DSSC. They had found that VO_2 improved the electrocatalytic behavior of the redox reaction between iodide and triiodide reactions, which might work as a substitute for expensive Pt electrodes due to their low cost, low-temperature processing, and excellent catalytic activity. Moreover, they reduced the cost of CE, but their efficiency is only about 1.25% [17]. They had alternatively prepared the V_2O_5 in two ways, one commercially purchased and the other by the hydrothermal method, and compared their CE properties for DSSC compatibility. They achieved efficiencies of 1.2% and 1.6% for commercial and hydrothermally prepared V_2O_5. In their paper, they also said that the properties of CEs could be made even better by tweaking their crystalline structure, surface shape, and ability to react with electrolytes. Therefore, V_2O_5 has potential as a viable alternative to platinum in terms of cost-effectiveness [18]. Also, Wu et al. [19] looked into Pt-free catalyst materials for CEs, which is seen as one of the most important steps to making DSSCs more efficient at converting energy and less expensive. They had prepared V_2O_3 composite catalysts that were successfully prepared and further applied to CEs as catalytic materials in the DSSC and achieved a PCE of 5.13% [19]. Gnanasekar and Nirmala Grace [18] have prepared the two-dimensional vanadium pentoxide nanosheets (V_2O_5 NS) by a simple hydrothermal method followed by calcinations at 350°C. In addition, the photocurrent voltage studies using V_2O_5 NS as the CE in DSSC achieved a PCE of 5.1%, which is much better than the conventional Pt CE's PCE of 7.4% under the same test conditions. This is a big improvement over previous report.

Also, this work encourages more in-depth studies to make the cheaper electrode VO_2 an alternative to Pt CE as a counter electrode for mass production. Vanadium-based oxides in the TMO family and vanadium-based compounds in MXenes have up to five-layer transition metals that have garnered significant attention in the realm of energy storage devices, including batteries and supercapacitors [20]. This is mostly due to their varied chemical motifs, layered structure,

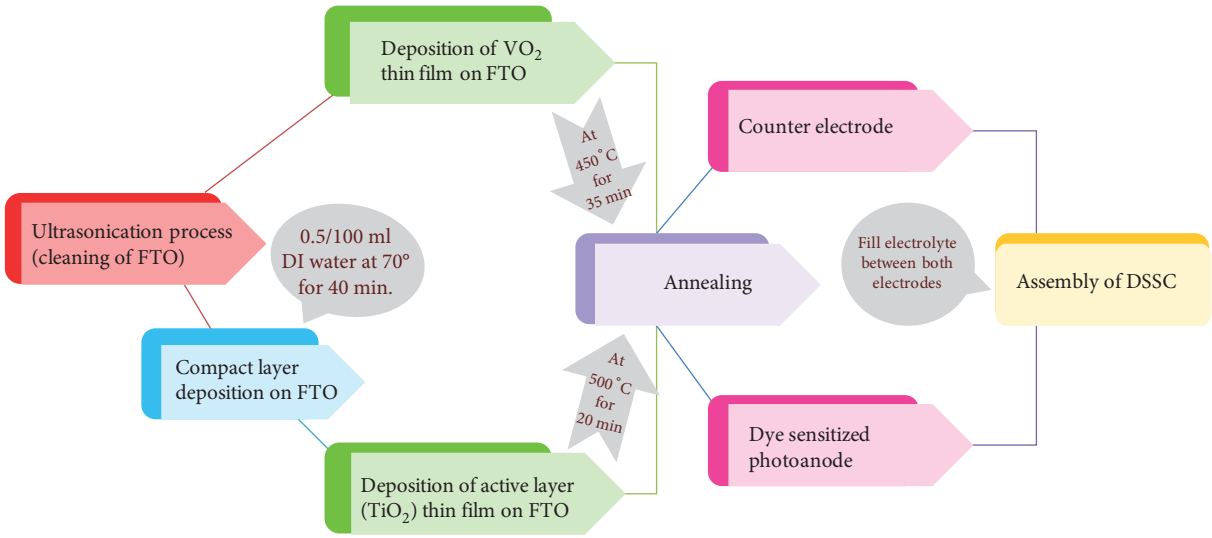

Figure 1: Schematic flowchart of a dye-sensitized solar cell.

substantial energy capacity, and moderate work functions [21]. From an economic perspective, it can be observed that the cost of raw materials for vanadium-based oxides, as calculated from the Sigma–Aldrich catalog, is ∼30 times lower than that of platinum with equivalent purity. The monoclinic form of vanadium oxide (VO_2) has garnered increased interest in the field of energy conversion and storage owing to its unique characteristics. These include its cost-effectiveness relative to platinum, high-energy storage capacity, moderate work function, and a first-order metal-to-insulator phase transition occurring at ∼68°C [19, 20]. Vanadium dioxide (VO_2) has not been used very often as a counter electrode (CE) in DSSC technology, according to the research that has been done [22, 23]. This study is the first to look into VO_2 (M1) as a counter electrode in DSSC technology, as far as what we know now allows. However, a close study of the existing literature shows that there are not many in-depth studies that look at the complex analysis of structural, crystalline, electrochemical, and photovoltaic properties. VO_2 has been talked about as a possible material for CE in DSSCs. Its shape, crystallinity, and catalytic properties can be changed in the literature. So, VO_2 was chosen for this study with two goals in mind: to improve its CE properties so that it could be used in industry and to learn more about the basic solid-state physics principles that govern its behavior.

The VO_2 paste was used as a counter electrode in this study. It was deposited on an FTO substrate and the device's overall photovoltaic performance was looked into. XRD and Rietveld refinement studies have been carried out to analyze the structure and crystalline properties. Furthering the study on the parameters linked to charge transport, the EIS is performed over a variety of voltages and extensively discussed along with their electrochemical performance.

2. Experimental Details

2.1. Materials. The Degussa P25 titanium dioxide nanopowder was acquired from Nanoshel India. The Vanadium dioxide (VO_2) nanopowder, fluorine-doped tin oxide (FTO) coated glass substrate with a sheet resistance of around 8–15 Ω/cm^2, potassium iodide (KI), iodine (I_2), acetonitrile and valeronitrile, ethyl cellulose, and α-terpineol were obtained from Sigma Aldrich and utilized without additional purification.

2.2. Vanadium Dioxide (VO_2) Paste Synthesis. In order to prepare the chemical paste of VO_2, the VO_2 (100 mg) powder, ethyl cellulose (16 mg), and a few drops of α-terpineol (a solvent) were used as the initial ingredients. First, all the ingredients were transferred to an agate, appropriately mixed with a pestle to form a homogeneous mixture, and then obtained into a smooth paste. All these steps were performed in ambient air at room temperature.

2.3. Device Structure and Fabrication. The schematic flowchart representations of DSSCs are demonstrated in Figure 1, which shows the complete process of device assembly. Initially, the small pieces of fluorine-doped tin oxide (FTO) coated glass substrate having sheet resistance ∼8–15 Ω/cm^2 are taken and cleaned with DI (deionized water), acetone, and 2–propanol, respectively, through an ultrasonication bath process for 30 min in each step. Subsequently, the preparation of a 10 mM solution of $TiCl_4$ in deionized water is conducted at a temperature of 70°C for a duration of 40 min. After making the solution, it is carefully washed with deionized water, which is then carefully deposited on the FTO substrate in the form of a thick layer. After that, the active layer is made with nanocrystalline TiO_2 paste that can be bought in stores and then put on the densely packed FTO substrates using the blade method. The substrate covered with TiO_2 was subjected to a sintering process at a temperature of 450°C for a duration of 35 min. Subsequently, the furnace is often subjected to a cooling process until it reaches the ambient temperature of the surrounding environment. After that, the electrode that had been made was carefully put into a solution that had a ruthenium-based dye (16 mg per 50 ml of 100% ethanol) in it. The electrode was then stored in a light-free environment at ambient temperature for a

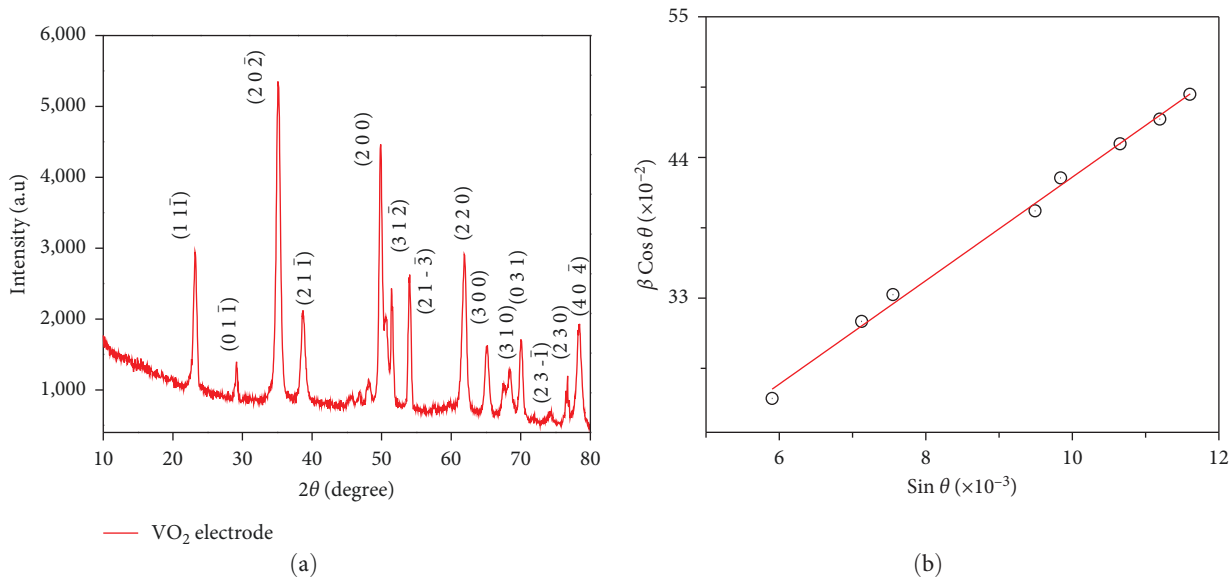

FIGURE 2: (a) X-ray diffraction graph pattern and (b) Williamsons and Hall (W–H) analysis of prepared VO_2 electrode.

duration of 22 hr. The dimensions of the active area of the photoanode used in the experiment are maintained at $1 \times 1\ cm^2$. The photoanode, which has been coated with dye, is subjected to a rinsing process using 1-propanol.

In contrast, the counter electrode is fabricated by applying VO_2 paste over the pristine FTO substrate using the Dr. Blade technique, resulting in a thickness of around 30 μm. Subsequently, the electrode that had been created underwent annealing at a temperature of 500°C for a duration of 20 min. The dye-sensitized photoanode and counter electrode are connected in a way that looks like a sandwich. A binder clip is attached to both sides of the substrate to make sure the sandwich is sealed securely. A solution containing electrolytes was prepared by mixing 0.90 g of potassium iodide (KI) and 0.150 g of iodine (I_2) in a 15 ml solution of acetonitrile. After that, the solution that was made was put into the space between the two electrodes, which finished building the DSSC device.

2.4. Characterization. An X-ray diffraction (XRD) analysis was performed using a Bruker Advance XRD instrument equipped with a Cu-Kα radiation source with a wavelength of 1.5406 Å. The purpose of this inquiry was to evaluate the crystal phase and crystalline size. The surface morphology of the photoanode was examined using a MIRA 3 TESCAN field emission scanning electron microscope. Additionally, elemental analysis and identification were performed using energy-dispersive X-ray spectroscopy (EDS). Thermo Scientifics' DXRxi Raman imaging microscope with a 532 nm excitation source was used to conduct the structural investigation. The current density and voltage (J–V) curves of fabricated cell were examined via Solar simulator (Verasol ORIEL LSS-7120) under AM 1.5 G irradiation. The fill factor is calculated from the J–V curves by the formula as follows:

$$FF = \frac{J_{max} \times V_{max}}{J_{sc} \times V_{oc}}, \quad (1)$$

where V_{max} and J_{max} represent the voltage and current density at the point of maximum power output, correspondingly, and J_{sc} and V_{oc} are represent the open circuit voltage (Voc) and short circuit current density, respectively.

The formula calculates the overall PCE (η) of cell as follows:

$$\eta = \frac{FF \times J_{sc} \times V_{oc}}{P_{in}}, \quad (2)$$

where P_{in} is assign for incident light (100 mW/cm^2), the cyclic voltammetry (CV) parameters are calculated with the help of Metrohm cyclic voltammetry instrument.

3. Results and Discussion

3.1. Characterization of Electrode. The prepared electrode undergoes several characterizations to seek their application in DSSC devices, as discussed in subsequent sections.

3.1.1. X-Ray Diffraction (XRD) Analysis. XRD analysis was used to look at the crystallinity and phase formation of the VO_2 counter electrode. The XRD pattern of VO_2 on the FTO substrate is shown in Figure 2(a). The pattern's peaks are clear and sharp, which suggests that the electrode sample has a high level of crystallinity [24]. The diffraction peaks were successfully correlated with the monoclinic phase of VO_2, as determined by the space group $C2/m$, as documented in JCPDS No. 01-082-0661 [24]. The Debye Scherrer equation was utilized to determine the crystallite size as part of the investigation into the crystalline characteristics.

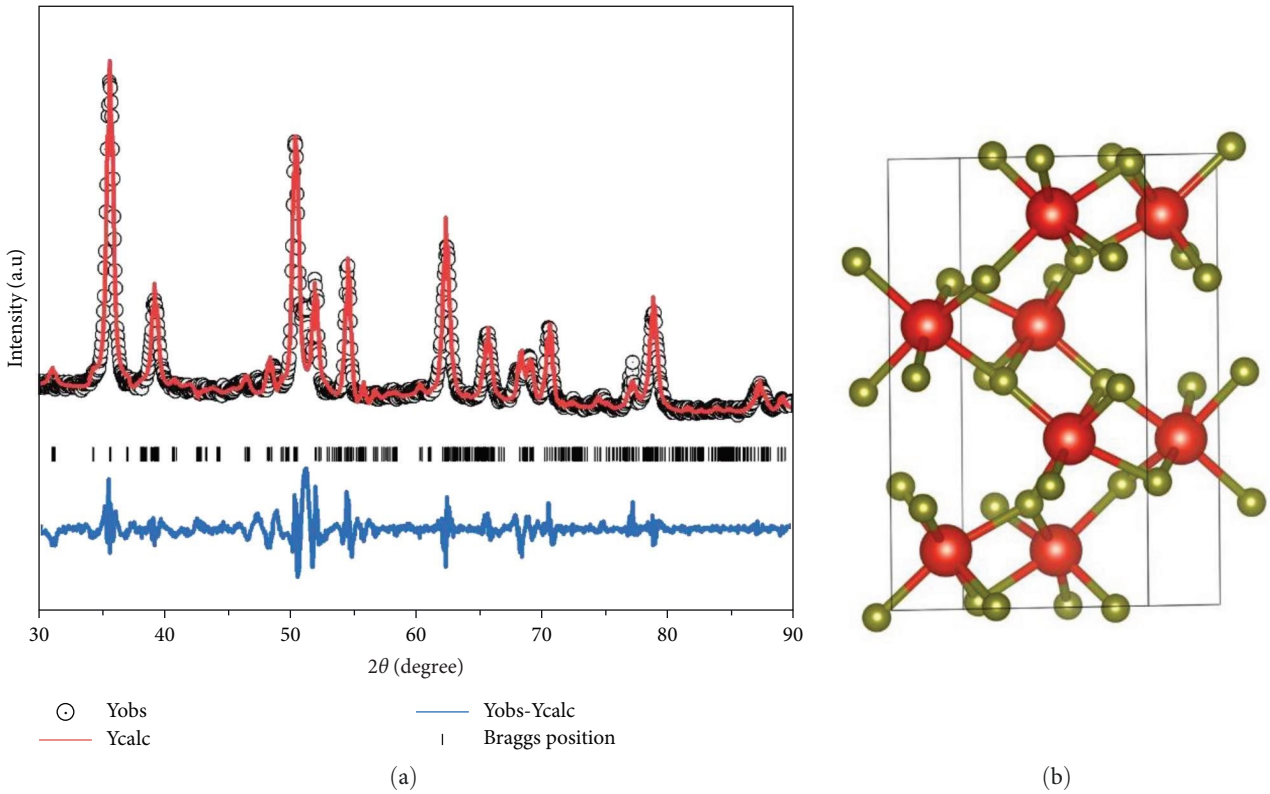

FIGURE 3: (a) Rietveld refinement pattern obtained from XRD data, (b) crystal structure obtained from CIF file after refinement (red ball represents atom V and the green represents O).

The observed widening of the peak width in XRD suggests that there may be a smaller crystallite size (D) and lattice strain. As per Debye Scherrer's findings, the full-width at half maximum (β) of an XRD peak, obtained from Gaussian fitting of the individual peaks, has been correlated with the size of the crystallite (D) using the following equation [25]:

$$D = \frac{k\lambda}{\beta \cos\theta}. \tag{3}$$

Within this equation, the variable k represents a constant possessing a numerical value of 0.91. The symbol λ denotes the X-ray wavelength, whereas θ signifies the angular position of an XRD peak. This study employed the greatest intensity peak of VO_2 nanoparticles to ascertain the size of the crystallites, which was determined to be 36.72 nm.

As previously mentioned, the presence of peak width has also been found to induce lattice strain. Hence, it might be argued that the accuracy of the crystallite size determined by the Debye–Scherrer equation is questionable. In addition, Williamson and Hall discovered a significant association between the variables β, D, and lattice strain (ε), and subsequently coined this approach as the Williamson–Hall plot. Based on the W–H plot, the crystallite size and lattice strain exhibited in each sample can be mathematically expressed by the following equation:

$$\beta \cos\theta = \frac{k\lambda}{D} + 4\varepsilon \sin\theta. \tag{4}$$

The W–H plot for the present sample has been generated and shown in Figure 2(b). The left part of above equation $\beta\cos\theta$ has been considered at y-axis and $4\sin\theta$ at x-axis suggests a linear equation ($y = mx + c$) with $m = \varepsilon$ and $c = \frac{k\lambda}{D}$. The current method finds the average crystalline dimension (D) by crossing over a linear regression line. The gradient of that line tells us about the lattice strain. The determined values for the crystallite size and lattice strain were 43.19 nm and 1.68×10^{-3}, respectively. The W–H plot has yielded a greater value for crystallite size compared to the value obtained using the Debye–Scherrer equation. Based on the analysis of Equation (3), it can be observed that the size of the crystallite exhibits an inverse relationship with β. Furthermore, since the component associated with lattice strain has been omitted from β, this leads to an increased value for the crystallite size [26]. Furthermore, XRD data have been utilized to derive an additional metric known as dislocation density (δ), in addition to the aforementioned parameters. The dislocation density quantifies the presence of defects and vacancies within the VO_2 sample. This parameter is computed by employing the Scherrer's formula to calculate the crystallite size [27].

$$\delta = \frac{1}{D^2}. \tag{5}$$

The dislocation density for the present sample has been found to be $5.36 \times 10^{14}/\mathrm{m}^2$. The numerical value of

Table 1: Rietveld refinement and structural parameters of VO_2 electrode sample.

Crystal structure	Monoclinic
Lattice parameter	
a (Å)	5.4266
b (Å)	5.0481
c (Å)	9.2000
Lattice angle (α, β, γ) (in degree)	(90, 90.331, 90)
Volume (Å^3)	251.9879
Rietveld refinement parameters	
R_p	8.37
R_{wp}	9.43
R_e	8.65
χ^2	4.3
$S = R_{wp}/R_e$	1.09

dislocation density suggests the presence of lattice defects and surface defects in the sample, which cause lattice strain.

However, to confirm the phase formation and determine the structural parameters more accurately, the XRD data have been further analyzed through Rietveld refinement using Full Prof software [28, 29]. The refined XRD graph pattern of the VO_2 electrode is shown in Figure 3(a). In the refined XRD pattern, the symbols show experimental data points (Yobs), the red line shows the XRD pattern generated through given input (Ycalc), the blue line shows the difference between the pattern observed and calculated, and the vertical line shows the Braggs position of VO_2 phase. The Rietveld refinement process has been carried out by taking crystal structure as monoclinic and space group $C2/m$. A sixth-order polynomial described the background with pseudo-Voight as a peak shape. All the parameters, such as lattice parameters, lattice angle, u, v, w, I_g, η_o, x were refined until they completely matched with the experimental pattern. The quality of fitting has been judged via calculating a parameter S with the formula, $S = R_{wp}/R_e$, where R_{wp} is the weighted profile factor and R_e is expected weighted profile reliability factors, respectively [30]. The crystal structure of the sample, as crystallized into monoclinic, has been obtained after refinement, as shown in Figure 3(b). All the structural parameters and Rietveld refinement parameters are given in Table 1.

It has been noticed that the value of parameter S found to be close to unity suggests that the parameters were relevant [26]. The lattice parameters obtained in this case were lower than the reported values in the literature [24]. The observed disparity in structural characteristics indicates the potential existence of surface defects, lattice faults, and other such imperfections. It is a well-known phenomenon that changes in processing parameters (such as time, temperature, etc.) result in slight differences in defects, resulting in variations in structural parameters too. The influence of flaws on optoelectronic and photovoltaic performance will be examined in the following section.

3.1.2. Surface Morphology Analysis. This photovoltaic system from DSSC works very differently depending on its shape and surface properties, which affect how much power it absorbs and how charges move between them. In this study, the surface morphology of counter electrode films composed of VO_2 was investigated using the field-emission scanning electron microscopy (FESEM). Figures 4(a) and 4(b) illustrate the surface morphology and energy dispersive spectrum of the VO_2 counter electrode. The morphology of the prepared electrode specimen indicates that the grains are in an irregular shape with a dense microstructure. It is also observed that the grains are agglomerated and having the irregularities in the sizes [23].

The surface's chemical homogeneity has been further recorded using energy-dispersive EDX, as shown in Figure 4(b). From Figure 4(b), elements V and O are found at the sample's surface, suggesting a uniform and homogeneous microstructure surface [31]. The weight percentages of V and O determined from the EDX spectrum are found to be 60.81% and 39.19%, which entirely agrees with their theoretical ratios present in VO_2 (V = 61.42%, O = 38.58%). Thus, it can be inferred that the surface of the prepared VO_2 counter electrode is homogenous.

3.1.3. Raman Analysis. Raman spectra are used to find the Raman active bands in a material in order to learn about its atomic-level symmetry and structure. Figure 5 shows the Raman spectrum of the VO_2 counter electrode.

The significant phonon peaks found between 100 and 1,100 cm^{-1} are possible distinctive vibrational modes of vanadium and oxygen that correlate to stretching, bending, and translational modes. The $(V_2O_2)_n$ chain translation's bending vibration modes, which correspond to the deformation of the bonding between various molecular units, peak at 146 cm^{-1} (B_{3g}, A_g symmetry) and 196 cm^{-1} (B_{1g} symmetry), where the detection is strongly correlated with the structure of the oxide layer. Additionally, the sharp and high peak at 146 cm^{-1} denotes long-range order in the vanadium oxide layer plane [32]. The bending vibration of the V═O bonds is connected with the peaks at 285 cm^{-1} (B_{2g}, B_{3g} symmetry) and 404 cm^{-1} (A_g symmetry). The peak at 485 cm^{-1} is attributed to the bending vibration of the V—O—V bond formed by doubly coordinated oxygen bridging with vanadium (A_g symmetry). The peak at 526 cm^{-1} (Ag symmetry) indicates the presence of a triply coordinated oxygen V—O stretching bond, which is brought about by the three pyramid systems' well-known edge-sharing oxygen atoms [24]. The double coordinated V—O stretching bond with a shared oxygen atom in the corner, which is common in the two-pyramid system, is what causes the peak at 703 cm^{-1} (B_{2g}, B_{3g} symmetry) [33]. The high-frequency peak at 996 cm^{-1} is caused by the terminal unshared oxygen V═O bond's in-phase stretching vibration. The vanadium oxide peaks that were found are similar to what was found before. That is, oxygen stoichiometric deviation had an effect on the oxide material's Raman spectra [34].

3.2. Characterization of Device

3.2.1. Cyclic Voltammetry Analysis. The cyclic voltammeter measurement is a powerful way to look at the electrocatalytic

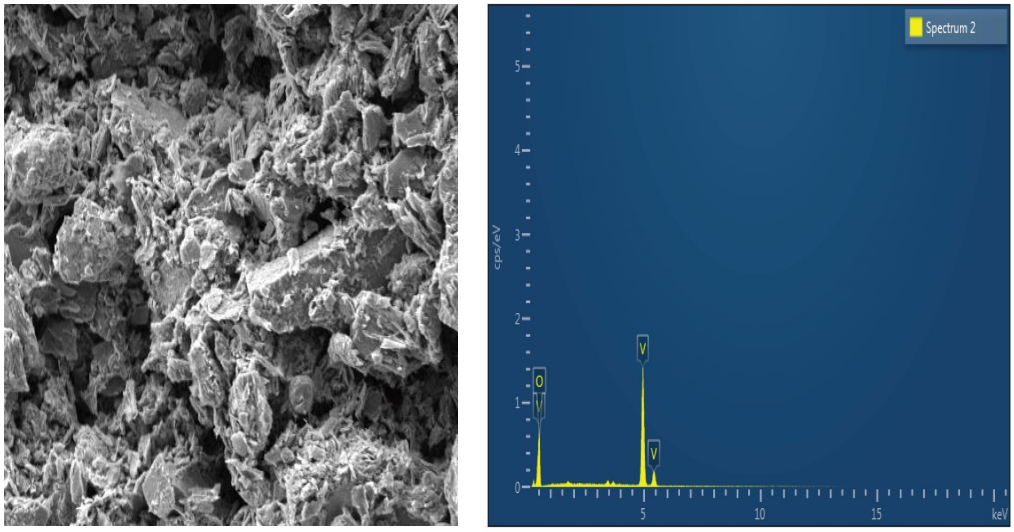

(a) (b)

Figure 4: (a) Structure morphology of prepared VO_2 thin film counter electrode and (b) EDX spectra of VO_2 thin film counter electrode.

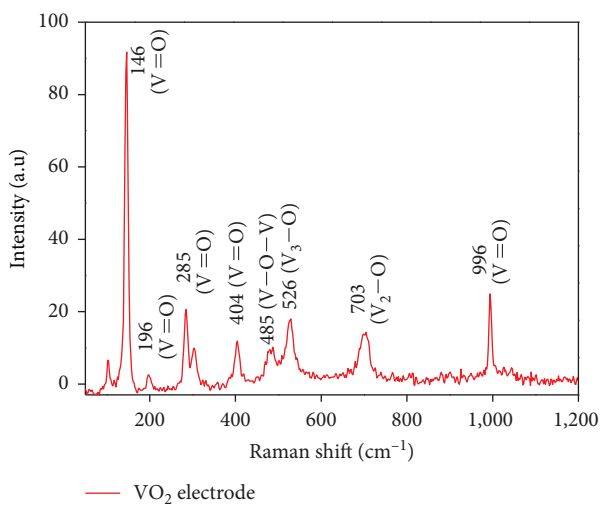

Figure 5: Raman spectra of VO_2-based counter electrode.

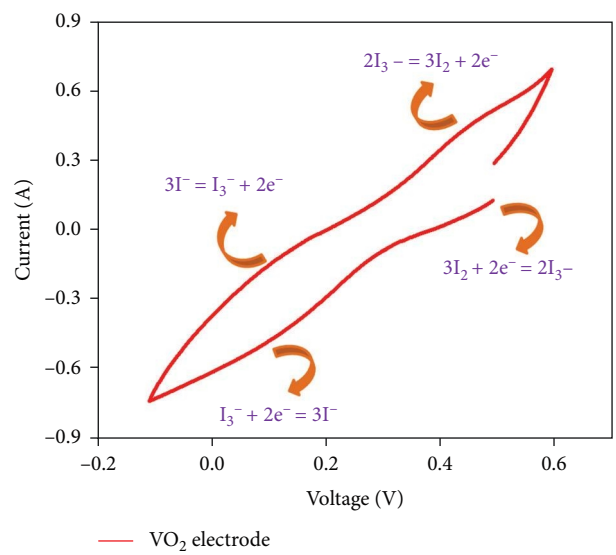

Figure 6: Cyclic voltammetry graph of VO_2 based CE recorded at the scan rate of 0.05 Vs − 1 in the acetonitrile electrolyte.

activity of a material toward the redox process and the speed at which electrons move between surfaces. Figure 6 represents the cyclic voltammetry curve achieved for VO_2 as a counter electrode in the three-electrode measurement system.

As a reference electrode [35], Pt wire is used as a counter electrode, and VO_2 coated on an FTO glass substrate is used as a working electrode. The electrode configuration is immersed in a solution containing iodide/tri-iodide, which serves as the electrolyte [32]. To make the electrolyte solution, acetonitrile is mixed with lithium chloride (LiCl) at a concentration of 0.1 M, lithium iodide (LiI) at a concentration of 10 mM, and iodine (I_2) at a concentration of 1 mM. The measurement was conducted using a scan rate of 50 mV within the potential range of −0.2 to 0.6 V. The conversion of the I^-/I^{3-} redox couple takes place through two reversible processes, which are indicated by the presence of two pairs of redox peaks on the FTO electrode covered with VO_2. The peaks found at the extreme left of the cyclic voltammetry curve are indicative of the oxidation process involving the conversion of I^-–I^{3-}. In contrast, the observed peak located at the far right of the spectrum corresponds to the reduction process wherein the conversion of I^{3-}–I^- takes place. During this process, the conversion of I^{3-} into I^- may occur, facilitated by the counter electrode, which has the ability to extract a small number of electrons from the external circuit. During this process, the released I^- ions can effectively facilitate the restoration of excited dye molecules to their ground state [23]. Peak current density and peak-to-peak separation (Epp) are the two crucial characteristics to recognize the

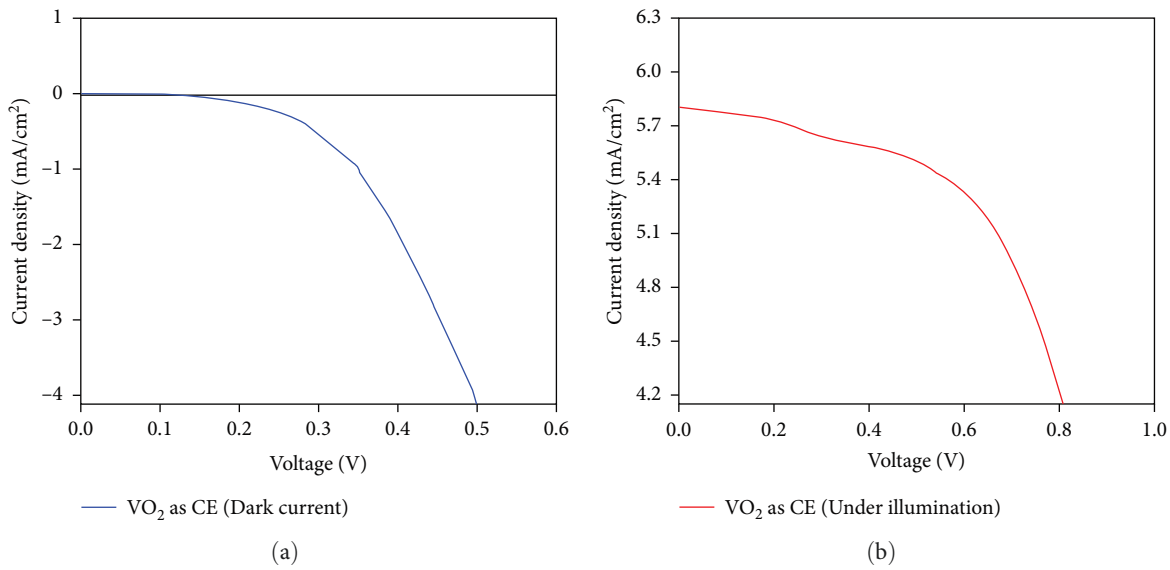

FIGURE 7: (a) The J–V curve under the illumination of VO_2 CE-based DSSC device under dark illumination (b) under illumination.

counter electrode's catalytic activity, and the following relation calculates them:

$$\text{Epp} = |\text{Ep(anodic)} - \text{Ep(cathodic)}|. \quad (6)$$

The Epp value of the VO_2 electrode is 0.36 V. The smaller Epp value indicates better catalytic activity for the electrode [36]. The cathodic and anodic peak current density of the VO_2 electrode was observed to be -4.72×10^{-3} and 4.09×10^{-3} mAcm^{-2}. The cathodic peak current density of VO_2 shows a shift toward negative values, indicating that the VO_2 electrode had a more excellent resistance with better catalytic activity [34].

3.2.2. Photovoltaic Performances of DSSCs. The photovoltaic parameters of the DSSCs device based on VO_2 as a counter electrode have been examined under simulated solar irradiation of 100 mWcm^{-2} (AM 1.5 G). The J–V curve of the DSSCs under dark and illumination conditions is illustrated in Figures 7(a) and 7(b), respectively.

The photovoltaic parameters of DSSC, such as current density, voltage, and fill factor with a corresponding PCE, including series and shunt resistances (R_s and R_{sh}), are measured under the illumination conditions given in Table 2. The fabricated DSSC represents an Voc of 0.80 V (the voltage obtained by the intercept at the voltage axis where the current is 0) under illumination conditions, while it is 0.50 V in the case of the dark condition [44]. The value of short circuit current density (Jsc) (is obtained at voltage 0 V) 5.85 mA/cm^2 under illumination from the J–V curve. The fill factor (FF) can be determined using the mathematical formula given by Equation (1). Using the values of maximum power point, V_{OC} and I_{SC}. The FF is calculated for the present sample and found to be 56.88% [44]. In addition to FF, the overall photo-conversion cell efficiency for the prepared electrode ($\eta = \text{FF} \times V_{OC} \times I_{SC}/P_{in}$) is calculated and found to be 2.69%–2.70%. The values of Voc, short-circuit current density, FF, and PCE for the present investigation are much higher than those in the report by Mutta et al. [23] At the same time, it is lower than the report by Gnanasekar et al. [32]. To lower the cost of producing DSSCs, Mutta et al. [23] used citric acid as a reducing agent to generate the sphere-like VO_2 (M1) polymorph in a single step. They found that VO_2 exhibits excellent electrocatalytic activity toward redox reactions, with a fivefold reduction in cost and a good energy conversion efficiency ratio (1.25%). However, Gnanasekar et al. [32] reported the post-electro-spun nanofiber of vanadium oxide wrapped in carbon (VO_2(M)/C). They also noted that at AM 1.5 G, VO_2(M)/C nanofiber CE achieves a typical DSSC PCE of 6.53% under 100 mV/cm^2 [45]. The outcomes showed that the electrocatalytic property of VO_2(M) nanofiber wrapped with carbon was enhanced, and the photon to photo-current conversion efficiency of the DSSC was boosted.

Compared to the report by Gnanasekar et al. [32], the efficiency in this case was lower. This could be because the shape, peak-to-peak separation (Epp), and other processing parameters were different [32]. The present result has been compared with the literature and summarized in Table 2. It has been noticed that several materials have been used as counter electrodes in DSSCs configurations. Among them, several materials show a higher value for J_{SC}, FF, and PCE compared to the present work. However, the value of Voc in the present work was observed to be remarkable higher compared to the reported values for other materials in the literature (Table 2). When it comes to PCE, graphene and CNT when used as CE in DSSCs have a higher photo-conversion efficiency than VO_2. This could be because of active surface interaction and the interfacial effect. Since the production of devices strongly depends on the cost of the electrode materials used in DSSC, the development of low-cost materials is in great demand for the commercialization of device fabrication. The production of graphene and CNT is more expensive than the production of VO_2, which implies that the use of VO_2 as

Table 2: Photovoltaic performance of various CEs material based DSSCs.

CE employed in DSSC	V_{OC} (V)	J_{SC} (mA/cm^2)	FF (%)	PCE (η) (%)	Reference
VO_2	0.80	5.85	56.88	2.70	This work
FeP	0.64	9.14	33.00	1.91	[37]
GO/RGO	0.61	0.77	19.20	0.09	[38]
Graphene	0.69	14.47	32.56	3.29	[39]
CNTs	0.73	15.27	69.00	8.03	[40]
SnO_2	0.52	9.81	36.01	1.84	[41]
WO_3	0.57	10.69	32.02	2.00	[42]
ZrN	0.73	8.20	22.00	1.20	[43]

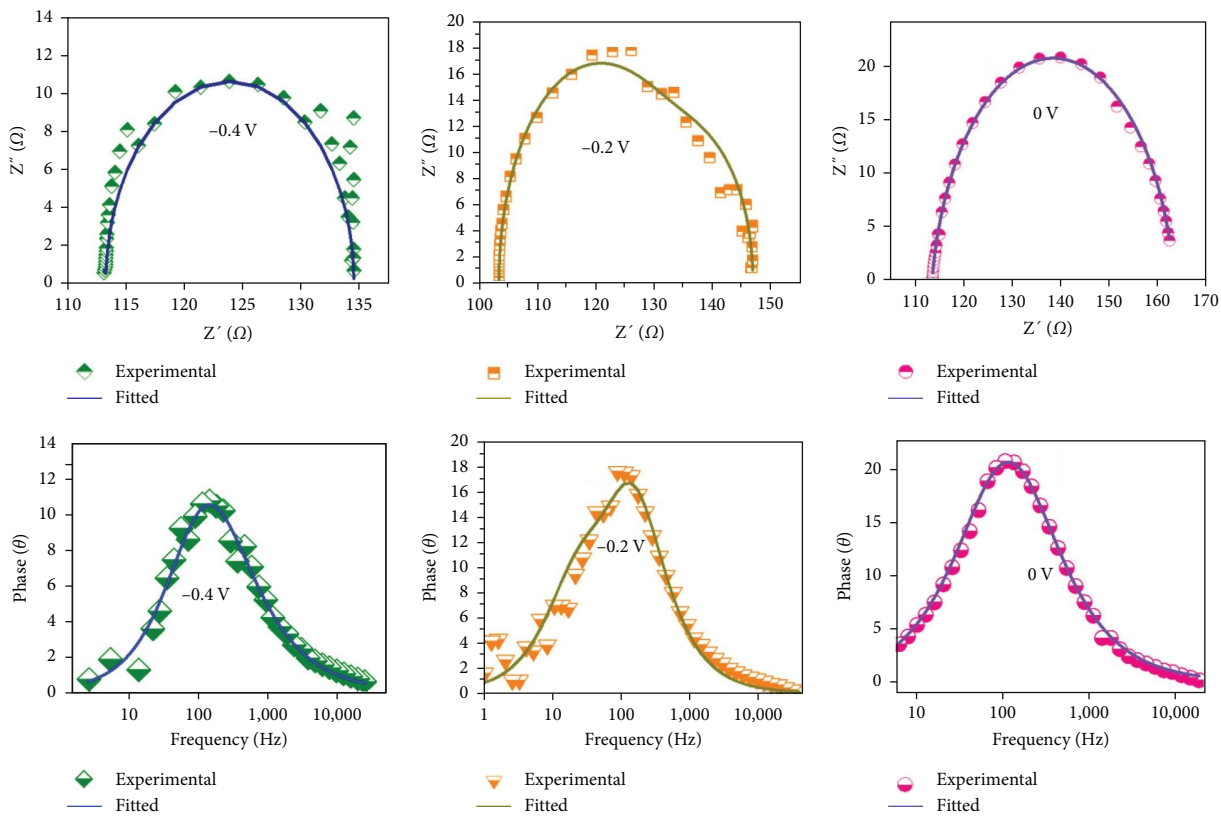

Figure 8: The Nyquist plots and bode plot of DSSC based on VO_2 CE at various voltages.

CE in DSSCs opens a new door for scientists to work on the fabrication of cost-effective DSSCs.

A critical factor in raising PCE, short circuit current density, and Voc is the series and shunt resistance. So, using the inverse slopes of the J–V curves recorded under illumination, the values of series resistance (Rs) and shunt resistance (Rsh) are determined, which are found to be 45.01 and 1,785 Ω, respectively. The amount of electrical and electrochemical losses experienced during DSSC operation is reflected in the FF [46]. Based on the photovoltaic parameters used as CEs [47], the devices that use VO_2 as the counter electrode show good photovoltaic performance. It is an excellent alternative to expensive platinum-based DSSCs with cost-effective factors. Moreover, the DSSC's photovoltaic performance is significantly impacted by VO_2 material. It is an excellent alternative to expensive platinum-based DSSC with cost-effective factors. Moreover, the DSSC's photovoltaic performance is significantly impacted by VO_2 material [48, 49].

This accomplishment opens the door for efficient research to increase the performance of this plentiful and affordable material, VO_2, by carefully tweaking the structure and cell architecture to meet future energy demand.

3.2.3. Electrochemical Impedance Performances of DSSC. To analyzing the internal impedance of solar systems like DSSC, electrochemical impedance spectroscopy (EIS) is a useful approach. It is helpful to analyze the electrocatalytic performance of the proposed CE toward the redox couple (I^{3-}, I^-) in detail [50]. The electrical characteristics of the device were analyzed with the help of EIS. Nyquist plots based on various applied voltages in the range of $-0.4 \leq V \leq 0$ volts are exhibited in Figure 8 with corresponding Bode plots [31].

Table 3: The capacitance and resistance values of an equivalent circuit of DSSC based on VO_2 counter electrode-based DSSC, corresponding to various voltages.

Sample	Applied voltage (V)	$R_S(\Omega)$	C_1(F)	C_2(F)	R_{CT} (Ω)	R_{RCE} (Ω)	Lifetime (τ) (sec)
	−0.4	92.86	2.683×10^{-07}	4.98×10^{-05}	19.33	22.34	1.130×10^{-03}
VO_2-CE based DSSC	−0.2	103.6	3.660×10^{-05}	5.02×10^{-03}	29.09	14.30	1.313×10^{-03}
	0	113.5	2.69×10^{-05}	6.91×10^{-05}	18.08	34.28	1.360×10^{-03}

All of the fitted curves match the experimental data when different voltages are applied in the dark at room temperature. As we can see in Figure 8, at 0 V, the fitted curve matches the measured data compared to other voltages—all impendence spectra at applied voltages except 0 V show some extra point values [11]. The table mentions all the corresponding impedance parameters extracted from the curves. The capacitance and resistance values of the equivalent circuit of DSSCs based on the VO_2 counter electrode are shown in Table 3.

As shown in Figure 8, the Bode plots show that frequency is shifted to a lower frequency region with the combination of TiO_2–VO_2 in the DSSC [51]. The lifetime of the electron (τ_e) is calculated from the maximum frequency of the low-frequency peak (f_{max}) value. Since f_{max} was inversely associated with the electron lifetime represented as follows [52]:

$$\tau_e = \frac{1}{2\pi f_{max}}. \quad (7)$$

The change in f_{max}, as shown in the above equation, indicates the reduction in the rate of recombination of charge involved in the DSSCs. The other parameters derived from the Bode plot, such as R_{CT} and R_{REC}, offer the resistive nature associated with charge transfer/transport at bulk and interfaces and the recombination resistance associated with recombination at the electrolyte and photocathode interfaces, respectively. Here, the electron lifetimes are high, which reflects a high rate of recombination between the photoanode and the electrolyte, as represented by R_{REC} [34]. There is strong evidence that the second circle in the impedance plots shows how the charge transfer process recombines at the interface, as shown by resistance due to charge transfer (R_{CT}) between TiO_2/Dye/Electrolyte/VO_2. Moreover, we calculate the charge collection efficiency by using the relation [53]:

$$\eta_C = \frac{1}{1+\frac{R_{CT}}{R_{REC}}}. \quad (8)$$

Furthermore, the charge collection efficiency is calculated with the help of Equation (8) and found to be 53.61%, 32.95%, and 65.46% at various applied voltages (−0.4, −0.2, and 0 V), respectively. According to these results and the examined optoelectronic performance, higher charge collection efficiency is due to decreased R_{CT} and higher charge recombination, which have a significant role in solid optoelectronic performance [54].

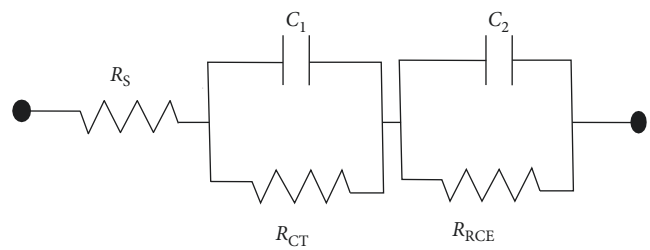

Figure 9: Electrical equivalent circuit for curve fitting obtained for VO_2 as CE in DSSC.

The obtained data have been reconfirmed by the best match data through simulation using the equivalent circuit model to the Nyquist plot and shown in Figure 9 for the purpose of interpreting the spectra of the measured data.

There is a Nyquist plot on the horizontal axis that shows the operating point of the electrical equivalent circuit. This plot shows the serial resistance (R_s) between conducting clips and a conducting substrate. In the impedance spectrum, the first half-circle (low) at high frequency (on the left) shows the resistance (R_{CT}) at the point where the counter electrode meets the electrolyte [51]. In contrast, the second semicircle at moderate frequency displays the resistance (R_{RCE}) at the interface between the photoanode and electrolyte [22, 55]. The internal series resistance of a DSSC is made up of two parts: R_{CT} is the sheet resistance of the conducting oxide substrates, and R_{RCE} is the diffusion resistance of I^{3-} ions in the electrolyte. This present work mainly focuses on electrolyte and counter electrodes [56]. This suggests that the electrolyte's ohmic losses and the interaction between the counter electrode film and electrolyte can be responsible for the internal series resistance values that were reported [32, 57]. It is clear from Nyquist plots that the R_{CT} magnitude of a VO_2-based DSSC is reasonably good, indicating that the VO_2-based DSSC's high-total internal impedance directly affects the electron transport mechanism in DSSCs.

4. Conclusion

In the end, the VO_2 material, which was used as a counter electrode in DSSCs, was able to make DSSCs that were both efficient and cost-effective. The structure, shape, and materials used to make the CE had an effect on the device's general characteristics and how it was used. FTIR, Raman, and absorption spectroscopy were used to confirm how the structure of the device changed and how the materials in it interacted with each other. XRD explains the crystalline properties, and refinement shows the monoclinic crystal structure of CEs. FESEM analysis indicates that the grains have a regular shape

with a dense microstructure. The electrochemical behavior of the material was recorded via cyclic voltammetry, which shows the VO_2 electrode had excellent resistance and better catalytic activity. The electrochemical impedance test shows that the VO_2 CE has a lot of electrocatalytic activity toward the iodide/triiodide redox electrolyte and a low charge transfer resistance that is the same as the Pt CE in the cell assembly. There is a very high Voc of 0.80 V and the DSSC PCE of VO_2 CE is 2.7% at AM 1.5 G and less than 100 mV/cm^2.The obtained results concluded that VO_2 exhibits improved electrocatalytic properties and increases the PCE of the DSSC. This accomplishment opens the door for efficient research to increase the performance of this fantastic and affordable material, VO_2, by carefully tailoring the structure and cell design to meet the coming energy demand.

Data Availability

The data used to support the findings of this study are included within the article.

Conflicts of Interest

The authors declare that they have no conflicts of interest.

Acknowledgments

The authors would like to be greatful for the financial and instrumental support from DST, India, under the CURIE program (grant no. SR/CURIE—Phase-III/01/2015(G)) and the Ministry of Human Resource Development (MHRD). The author, Upendra Kumar, acknowledges the Science and Engineering Research Board (SERB) for the research grant (File No.: SERB/EEQ/2021/000132).

References

[1] J. Li and D. Chu, "Energy band engineering of metal oxide for enhanced visible light absorption," in *Multifunctional Photocatalytic Materials for Energy*, pp. 49–78, Woodhead Publishing in Materials, 2018.

[2] R. F. Mansa, A. R. A. Yugis, K. S. Liow et al., "A brief review on photoanode, electrolyte, and photocathode materials for dye-sensitized solar cell based on natural dye photosensitizers," in *Developments in Sustainable Chemical and Bioprocess Technology*, pp. 313–319, Springer, Boston, MA, 2013.

[3] H. Fujiwara and M. Kondo, "Effects of *a*-Si: H layer thicknesses on the performance of *a*-Si: H/*c*-Si heterojunction solar cells," *Journal of Applied Physics*, vol. 101, no. 5, Article ID 54516, 2007.

[4] J. Gong, J. Liang, and K. Sumathy, "Review on dye-sensitized solar cells (DSSCs): fundamental concepts and novel materials," *Renewable and Sustainable Energy Reviews*, vol. 16, no. 8, pp. 5848–5860, 2012.

[5] S. R. Wenham, M. A. Green, M. E. Watt, R. Corkish, and A. Sproul, *Applied Photovoltaics*, Routledge, London, 2013.

[6] K. Ranabhat, L. Patrikeev, A. Antal'evna-Revina, K. Andrianov, V. Lapshinsky, and E. Sofronova, "An introduction to solar cell technology," *Journal of Applied Engineering Science*, vol. 14, no. 4, pp. 481–491, 2016.

[7] K. Sharma, V. Sharma, and S. S. Sharma, "Dye-sensitized solar cells: fundamentals and current status," *Nanoscale Research Letters*, vol. 13, Article ID 381, 2018.

[8] J. Gong, K. Sumathy, Q. Qiao, and Z. Zhou, "Review on dye-sensitized solar cells (DSSCs): advanced techniques and research trends," *Renewable and Sustainable Energy Reviews*, vol. 68, Part 1, pp. 234–246, 2017.

[9] A. W. Copeland, O. D. Black, and A. B. Garrett, "The photovoltaic effect," *Chemical Reviews*, vol. 31, no. 1, pp. 177–226, 1942.

[10] B. Ratier, J.-M. Nunzi, M. Aldissi, T. M. Kraft, and E. Buncel, "Organic solar cell materials and active layer designs—improvements with carbon nanotubes: a review," *Polymer International*, vol. 61, no. 3, pp. 342–354, 2012.

[11] C. C. Raj and R. Prasanth, "A critical review of recent developments in nanomaterials for photoelectrodes in dye sensitized solar cells," *Journal of Power Sources*, vol. 317, pp. 120–132, 2016.

[12] K. Zhang, C. Qin, X. Yang et al., "High-performance, transparent, dye-sensitized solar cells for see-through photovoltaic windows," *Advanced Energy Materials*, vol. 4, no. 11, Article ID 1301966, 2014.

[13] A. Carella, F. Borbone, and R. Centore, "Research progress on photosensitizers for DSSC," *Frontiers in Chemistry*, vol. 6, Article ID 481, 2018.

[14] D. Wei, "Dye sensitized solar cells," *International Journal of Molecular Sciences*, vol. 11, no. 3, pp. 1103–1113, 2010.

[15] K. Rokesh, A. Pandikumar, and K. Jothivenkatachalam, "Dye sensitized solar cell: a summary," *Materials Science Forum*, vol. 771, pp. 1–24, 2013.

[16] J. Xia, C. Yuan, and S. Yanagida, "Novel counter electrode V_2O_5/Al for solid dye-sensitized solar cells," *ACS Applied Materials & Interfaces*, vol. 2, no. 7, pp. 2136–2139, 2010.

[17] G. R. Mutta, S. R. Popuri, M. Vasundhara et al., "Facile hydrothermal synthesis of economically viable VO_2(M1) counter electrode for dye sensitized solar cells," *Materials Research Bulletin*, vol. 83, pp. 135–140, 2016.

[18] S. Gnanasekar and A. Nirmala Grace, "V_2O_5 nanosheets as an efficient, low-cost Pt-free alternate counter electrode for dye-sensitized solar cells," *ChemNanoMat*, vol. 8, no. 2, Article ID e202100382, 2022.

[19] K. Wu, D. Yang, J. Guo et al., "Performance of V_2O_3@C composites via a sol–gel precursor assisted by soluble starch as Pt-free counter electrodes for dye sensitized solar cells," *Solar Energy*, vol. 213, pp. 126–135, 2021.

[20] T. Ramachandran, F. Hamed, Y. A. Kumar, R. K. Raji, and H. H. Hegazy, "Multifunctional covalent–organic frameworks (COFs)-2D MXenes composites for diverse applications," *Journal of Energy Storage*, vol. 73, Part D, Article ID 109299, 2023.

[21] T. Ramachandran, F. Hamed, R. K. Raji et al., "Enhancing asymmetric supercapacitor performance with $NiCo_2O_4$–NiO hybrid electrode fabrication," *Journal of Physics and Chemistry of Solids*, vol. 180, Article ID 111467, 2023.

[22] S. Thomas, T. G. Deepak, G. S. Anjusree, T. A. Arun, S. V. Nair, and A. S. Nair, "A review on counter electrode materials in dye-sensitized solar cells," *Journal of Materials Chemistry A*, vol. 2, no. 13, pp. 4474–4490, 2014.

[23] G. R. Mutta, S. R. Popuri, M. Maciejczyk et al., "V_2O_5 as an inexpensive counter electrode for dye sensitized solar cells," *Materials Research Express*, vol. 3, no. 3, Article ID 035501, 2016.

[24] Z. Fan, L. Jia, C. Lin et al., "Enhanced electrochemical performance of vanadium dioxide (B) nanoflowers with

graphene nanoribbons support," *RSC Advances*, vol. 6, no. 16, pp. 13297–13302, 2016.

[25] R. Suriakarthick, M. Senthil Pandian, P. Ramasamy et al., "Solvothermal synthesis, structural and transport properties of polycrystalline copper tin selenide for thermoelectric applications," *Inorganic Chemistry Communications*, vol. 140, Article ID 109491, 2022.

[26] A. Kumar, B. Khan, V. Yadav, A. Dixit, U. Kumar, and M. K. Singh, "Rietveld refinement, optical, dielectric and ac conductivity studies of Ba-doped $SrSnO_3$," *Journal of Materials Science: Materials in Electronics*, vol. 31, pp. 16838–16848, 2020.

[27] A. Ahmed, M. A. Jalil, M. M. Hossain et al., "A PEDOT:PSS and graphene-clad smart textile-based wearable electronic Joule heater with high thermal stability," *Journal of Materials Chemistry C*, vol. 8, no. 45, pp. 16204–16215, 2020.

[28] Q. Kang, Y. Zhang, S. Bao, and G. Zhang, "Eco-friendly synthesis of VO_2 with stripped pentavalent vanadium solution extracted from vanadium-bearing shale by hydrothermal process in high conversion rate," *Royal Society Open Science*, vol. 6, no. 2, Article ID 181116, 2019.

[29] U. Kumar, J. Ansaree, and S. Upadhyay, "Structural and optical characterizations of BaSnO3," "nanopowder synthesized by aqueous sol–gel method," *Processing and Application of Ceramics*, vol. 11, no. 3, pp. 177–184, 2017.

[30] U. Kumar and S. Upadhyay, "Investigation of structural, optical and electrical properties of Sr_2 SnO_4, $Sr_{1.99}$ $Eu_{0.01}$ SnO_4 and Sr_2 $Sn_{0.99}$ $Eu_{0.01}$ O_4 ruddlesden popper oxide," *Materials Research Express*, vol. 6, no. 5, Article ID 055805, 2019.

[31] A. Upadhyaya, C. M. Singh Negi, A. Yadav, S. K. Gupta, and A. S. Verma, "I-V and impedance characterization of a solution processed perovskite based heterojunction photodetector," *Superlattices and Microstructures*, vol. 122, pp. 410–418, 2018.

[32] S. Gnanasekar, P. Kollu, S. K. Jeong, and A. N. Grace, "Pt-free, low-cost and efficient counter electrode with carbon wrapped VO_2(M) nanofiber for dye-sensitized solar cells," *Scientific Reports*, vol. 9, Article ID 5177, 2019.

[33] H. Cheema, V. Yadav, R. S. Maurya et al., "Structural, optical and electrical properties of Mn-doped $ZnFe_2O_4$ synthesized using sol–gel method," *Journal of Materials Science: Materials in Electronics*, vol. 32, pp. 23578–23600, 2021.

[34] M. Lee, S. K. Balasingam, Y. Ko et al., "Graphene modified vanadium pentoxide nanobelts as an efficient counter electrode for dye-sensitized solar cells," *Synthetic Metals*, vol. 215, pp. 110–115, 2016.

[35] T. Ramachandran, A.-H. I. Mourad, R. K. Raji et al., "KOH mediated hydrothermally synthesized hexagonal-$CoMn_2O_4$ for energy storage supercapacitor applications," *International Journal of Energy Research*, vol. 46, no. 12, pp. 16823–16838, 2022.

[36] D. Kishore Kumar, J. Loskot, J. Kříž et al., "Synthesis of SnSe quantum dots by successive ionic layer adsorption and reaction (SILAR) method for efficient solar cells applications," *Solar Energy*, vol. 199, pp. 570–574, 2020.

[37] A. Yildiz, T. Chouki, A. Atli et al., "Efficient iron phosphide catalyst as a counter electrode in dye-sensitized solar cells," *ACS Applied Energy Materials*, vol. 4, no. 10, pp. 10618–10626, 2021.

[38] M. Y. A. Rahman, A. S. Sulaiman, A. A. Umar, and M. M. Salleh, "Dye-sensitized solar cell (DSSC) utilizing reduced graphene oxide (RGO) films counter electrode: effect of graphene oxide (GO) content," *Journal of Materials Science: Materials in Electronics*, vol. 28, pp. 1674–1678, 2017.

[39] D. W. Zhang, X. D. Li, H. B. Li et al., "Graphene-based counter electrode for dye-sensitized solar cells," *Carbon*, vol. 49, no. 15, pp. 5382–5388, 2011.

[40] J. G. Nam, Y. J. Park, B. S. Kim, and J. S. Lee, "Enhancement of the efficiency of dye-sensitized solar cell by utilizing carbon nanotube counter electrode," *Scripta Materialia*, vol. 62, no. 3, pp. 148–150, 2010.

[41] M. Wu, Y. Wang, X. Lin, A. Hagfeldt, and T. Ma, "An autocatalytic factor in the loss of efficiency in dye-sensitized solar cells," *ChemCatChem*, vol. 4, no. 9, pp. 1255–1258, 2012.

[42] Y. Wang, C. Zhao, M. Wu, W. Liu, and T. Ma, "Highly efficient and low cost Pt-based binary and ternary composite catalysts as counter electrode for dye-sensitized solar cells," *Electrochimica Acta*, vol. 105, pp. 671–676, 2013.

[43] M. Wu, X. Lin, Y. Wang et al., "Economical Pt-free catalysts for counter electrodes of dye-sensitized solar cells," *Journal of the American Chemical Society*, vol. 134, no. 7, pp. 3419–3428, 2012.

[44] V. Yadav, C. M. S. Negi, D. K. Kumar, and S. K. Gupta, "Fabrication of eco-friendly, low-cost dye sensitized solar cells using harda fruit-based natural dye," *Optical Materials*, vol. 122, Part B, Article ID 111800, 2021.

[45] M. J. Morgan, G. Jakovidis, and I. McLeod, "An experiment to measure the *I–V* characteristics of a silicon solar cell," *Physics Education*, vol. 29, no. 4, Article ID 252, 1994.

[46] W. A. Ayalew and D. W. Ayele, "Dye-sensitized solar cells using natural dye as light-harvesting materials extracted from *Acanthus sennii chiovenda* flower and *Euphorbia cotinifolia* leaf," *Journal of Science: Advanced Materials and Devices*, vol. 1, no. 4, pp. 488–494, 2016.

[47] M. Singh, R. Kurchania, R. J. Ball, and G. D. Sharma, "Efficiency enhancement in dye sensitized solar cells through step wise cosensitization of TiO_2 electrode with N719 and metal free dye," *Indian Journal of Pure & Applied Physics*, vol. 54, pp. 656–664, 2016.

[48] J. Ouyang, "Applications of carbon nanotubes and graphene for third-generation solar cells and fuel cells," *Nano Materials Science*, vol. 1, no. 2, pp. 77–90, 2019.

[49] J. Liu, Y. Li, S. Yong, S. Arumugam, and S. Beeby, "Flexible printed monolithic-structured solid-state dye sensitized solar cells on woven glass fibre textile for wearable energy harvesting applications," *Scientific Reports*, vol. 9, Article ID 1362, 2019.

[50] V. Yadav, S. Chaudhary, S. K. Gupta, and A. S. Verma, "Synthesis and characterization of TiO_2 thin film electrode based dye sensitized solar cell," *East European Journal of Physics*, no. 3, pp. 129–133, 2020.

[51] A. Yadav, A. Upadhyaya, S. K. Gupta, A. S. Verma, and C. M. Singh Negi, "Solution processed graphene as electron transport layer for bulk heterojunction based devices," *Superlattices and Microstructures*, vol. 120, pp. 788–795, 2018.

[52] V. Saini, O. Abdulrazzaq, S. Bourdo et al., "Structural and optoelectronic properties of P3HT-graphene composites prepared by *in situ* oxidative polymerization," *Journal of Applied Physics*, vol. 112, no. 5, Article ID 054327, 2012.

[53] S. Chaudhary, V. Yadav, C. M. Singh Negi, and S. K. Gupta, "Active layer thickness dependence of optoelectronic performance in $CH_3NH_3PbI_3$ perovskite-based planar heterojunction photodiodes," *Optical Materials*, vol. 106, Article ID 109960, 2020.

[54] P. Bhatt, K. Pandey, P. Yadav et al., "Investigating the charge carrier transport within the hole-transport material free perovskite solar cell processed in ambient air," *Solar Energy Materials and Solar Cells*, vol. 140, pp. 320–327, 2015.
[55] E. von Hauff, "Impedance spectroscopy for emerging photovoltaics," *The Journal of Physical Chemistry C*, vol. 123, no. 18, pp. 11329–11346, 2019.
[56] W. Ghann, H. Kang, T. Sheikh et al., "Fabrication, optimization and characterization of natural dye sensitized solar cell," *Scientific Reports*, vol. 7, Article ID 41470, 2017.
[57] D. K. Kumar, S. K. Swami, V. Dutta, B. Chen, N. Bennett, and H. M. Upadhyaya, "Scalable screen-printing manufacturing process for graphene oxide platinum free alternative counter electrodes in efficient dye sensitized solar cells," *FlatChem*, vol. 15, Article ID 100105, 2019.